AIAA JOURNAL
Vol. 33, No. 8, August 1995

Numerical Vorticity Confinement for Vortex–Solid Body Interaction Problems

Clin M. Wang*
Flow Analysis, Inc., Tullahoma, Tennessee 37388
and
John S. Steinhoff† and Yonghu Wenren‡
University of Tennessee Space Institute, Tullahoma, Tennessee 37388

A new numerical method based on adding a term to the Euler/Navier–Stokes equations has demonstrated that it can effectively treat vortex-dominated flows using low-order numerical schemes and coarse grids. With the technique, numerical diffusion introduced by convection schemes can be eliminated when solving the modified flow governing equations. The modification of the velocity field, which conserves the total vorticity, essentially convects the vorticity toward its local extreme to offset the numerical diffusion. This method preserves the vortex structure even when vortices travel through a coarse grid region. The method is implemented separately with two distinctive basic solvers: a Navier–Stokes flow solver based on a vorticity–velocity formulation and an Euler solver based on a velocity–pressure formulation. Problems presented in this paper include airfoil dynamic stall, vortex–airfoil interaction, and vortex–fuselage interactions.

Introduction

BECAUSE of the complexity of flowfields around rotorcraft and the lack of efficient numerical procedures to analyze these flows, the prediction of rotorcraft aerodynamics is today very difficult and inadequate. This is mainly because the flow is highly unsteady and strong, concentrated vortices are shed from rotor blades, which have dominant effects on many aspects of the aerodynamics. These problems include blade retreating side dynamic stall, blade–vortex interactions, and rotor–airframe interactions. Because of the importance of these vortex-dominated flows, many researchers have attempted to find viable numerical methods for their prediction over the past several decades. In spite of these efforts, accurate and efficient methods for the computation of general rotorcraft (or other) flows with strong, concentrated vortices still do not exist.

Conventional computational methods for vortex-dominated flows can be grouped into two classes: Eulerian and Lagrangian. In the Eulerian approach, body-fixed grids can be used effectively with discretized flow equations for flows at low Reynolds number where shed vorticity is spread over a rather wide region. However, for large Reynolds number flows, where this region is thin, it is very difficult to include the number of grid points required for adequate resolution.

There are two Eulerian numerical techniques that have provided some improvement in treating the thin vortical regions: high-order discretization and adaptive grid schemes. Examples of these approaches to solve for a vortex impinging on an airfoil include the use of a fifth-order discretization for the Navier–Stokes equations together with a fine, regular grid in the entire domain.[1] This requires a large amount of computing since the grid must be fairly fine, even though fairly efficient implicit solvers can be used since the grid is regular. Adaptive grid schemes have been used for problems involving, for example, a vortex impinging on an airfoil,[2] a steady vortex shed at the tip of a straight wing,[3] and a vortex sheet shed from the leading edge of a delta wing.[4] It can be shown that, despite the adaptive embedding of extra grid points in the vortical region, these methods apparently still are not able to capture the shed vortex without having it spread over a region much larger than measured in experiments. In addition, the unstructured and moving grids require complex logic and bookkeeping. Without regular grids, conventional and efficient implicit methods usually cannot be used.

In the Lagrangian approach, use is made of the fact that the internal structure of vortical regions, such as vortex sheets, are not important since the dimensions of these structures are small compared with other dimensions of the problem. As long as the centroid surfaces of these vortex sheets are accurately computed, together with the total vorticity surrounding each point on the centroid surface, the overall flow solution will be accurate. An ad hoc structure can then be used instead of resorting to a detailed, high-resolution Navier–Stokes solver. Usually a "spreading" function is specified that, effectively, defines the internal structure of vortical regions treated with this approach. For these reasons, some of the most efficient methods for treating the thin vortical flows currently involve Lagrangian marker-based schemes, where vorticity or circulation is assigned to individual markers that convect through the flowfield. These methods, in the form of "vortex lattice" or "vortex blob" techniques for incompressible flows[5] and "vortex embedding" techniques for compressible flows,[6] entail representation of vortex sheets or vortex filaments by surfaces or lines defined by markers.

Unfortunately, there are disadvantages to these Lagrangian methods. Since the vortical regions are defined by connected sets of markers, the topology of each region should be known beforehand so that suitable arrays of markers can be computationally defined. In general, the vortical regions may interact with solid surfaces and their topology may change. This requires new specifications of the markers and reconnection. In addition, vortical regions cannot easily be made to merge in a natural way if they are defined by markers. Lagrangian methods that use large numbers of basic markers with overlapping structure also appear to require information on the locations of vortical regions for the allocation of markers.

The computational technique presented here is fundamentally different from the previously described methods in that it involves adding a term to the continuum flow equations before discretization and therefore modifying the basic Euler/Navier–Stokes equations. With the added term, the flow equations admit solutions with concentrated vortices that can convect without spreading, even if the basic equations have diffusive terms. For this reason, simple, low-order diffusive numerical schemes can be used to discretize and solve the modified flow equations, without resulting in vortices that spread as they convect. The present approach is similar to shock

Presented as Paper 93-3343 at the AIAA Applied Aerodynamics Conference, Monterey, CA, Aug. 9–11, 1993; received Feb. 22, 1994; revision received Jan. 4, 1995; accepted for publication Jan. 4, 1995.

*Senior Scientist. Member AIAA.
†Associate Professor; also Senior Scientist, Flow Analysis, Inc., Tullahoma, TN 37388. Member AIAA.
‡Research Assistant; also Associate Scientist, Flow Analysis, Inc., Tullahoma, TN 37388. Member AIAA.

capturing where the detailed internal dynamics of shocks are not computed, but rather a modified set of equations is solved that results in a shock spread over a few number of grid cells. The resulting internal structure satisfies conservation laws in integral form. Some aspects of the present "vorticity confinement" method are presented in Refs. 7 and 8.

The new method has the flexibility and generality of standard Euler/Navier–Stokes methods but treats vortical regions without numerical diffusion as they convect through the flow even in regions where the computational grid is relatively coarse. The vorticity confinement method uses only fixed, Eulerian grid with no markers and no special logic concerning shed vortices. It consists, basically, of a velocity correction to be applied at each time step at grid points where velocity values are obtained by the basic solver. This correction is applied only in relatively coarse grid regions, as vortical fluid is convecting. As such, it is capable of being used in conjunction with conventional Euler/Navier–Stokes methods that can serve as the basic flow solver.

In the present study, the new method is coupled to an existing incompressible Navier–Stokes code using vorticity–velocity formulation to study dynamic stall and vortex–airfoil interaction problems. The method is also used with an incompressible Euler flow solver developed recently by the present authors using velocity–pressure formulation. This solver is used for the study of vortex–fuselage interaction problems.

Vorticity Confinement Method

The method involves adding a term to the momentum part of the continuum Euler/Navier–Stokes equations. The extra confinement term is local and simple to discretize. It is nonzero only within the vortical regions and does not change the total vorticity or mass within those regions. The technique is applicable to general compressible and incompressible flows (for supersonic flows additional considerations are required). For conciseness, the vorticity confinement method is described here for incompressible flow using the velocity–pressure formulation. For a general unsteady flow, we can represent the solution as approximately satisfying the following equations:

$$\nabla \cdot \boldsymbol{q} = 0 \tag{1}$$

$$\partial_t \boldsymbol{q} = -(\boldsymbol{q} \cdot \nabla)\boldsymbol{q} + \nabla p/\rho + \mu \nabla^2 \boldsymbol{q} + \epsilon \boldsymbol{s} \tag{2}$$

where $\boldsymbol{q}$ is the velocity vector, t is time, and p and ρ represent pressure and density, respectively. The diffusion term represents an effective diffusivity of the basic numerical solution method. The additional term, $\epsilon \boldsymbol{s}$ is the confinement term where the numerical coefficient ϵ controls the size of the convecting vortical regions. The confinement term has the form

$$\boldsymbol{s} = -\boldsymbol{n} \times \boldsymbol{\omega} \tag{3}$$

$$\boldsymbol{n} = \nabla \eta / |\nabla \eta| \tag{4}$$

where

$$\boldsymbol{\omega} = \nabla \times \boldsymbol{q} \tag{5}$$

is the vorticity vector and η is a scalar field that has a local minimum on the centroid of the vortical region:

$$\eta = -|\boldsymbol{\omega}| \tag{6}$$

For the confinement term, $\boldsymbol{n}$ is a unit vector pointing away from the centroid of the vortical region, and the term serves to convect $\boldsymbol{\omega}$ back towards the centroid as $\boldsymbol{\omega}$ diffuses away. This convection increases the diffusion and a steady-state form results when the two terms become balanced. It is noted that steady-state solutions exist, for any positive value of ϵ. It appears to be better to discretize the set of Eqs. (1) and (2) for problems that have thin, well-behaved vorticity distribution, even in the presence of the numerical diffusion, than to discretize the unmodified equations that only admit vorticity regions that continue to spread, if there is any numerical diffusion.

An important feature of the vorticity confinement method is that the velocity correction is limited to the vortical region only. The correction effectively convects vorticity back towards the local extreme of the vortical region. The total change induced by the confinement term in mass δI_ρ and vorticity δI_ω can be expressed by

$$\delta I_\rho = \epsilon \int_{R_\omega} \nabla \cdot \boldsymbol{s}\, dV \tag{7}$$

$$\delta I_\omega = \epsilon \int_{R_\omega} \nabla \times \boldsymbol{s}\, dV \tag{8}$$

The integration is performed on the vortical domain R_ω. It is simple to show that $\delta I_\rho = 0$ and $\delta I_\omega = 0$ by using Eq. (3), i.e., the confinement term conserves mass and the total vorticity. Conservation properties involving fluid momentum are discussed in Ref. 9.

The effect of the confinement term can be illustrated for a simple two-dimensional flow where an isolated axisymmetric vortex moves in a uniform flow. If $\boldsymbol{r}$ is a position vector defined with respect to the center of the vortex, then Eqs. (4) and (6) will give

$$\boldsymbol{n} = \boldsymbol{r}/r \tag{9}$$

where $r = |\boldsymbol{r}|$. The velocity of the flowfield can be represented by

$$\boldsymbol{q} = \boldsymbol{q}_\infty + T(r, t)\boldsymbol{e}_\theta \tag{10}$$

where $\boldsymbol{q}_\infty$ is the uniform velocity, T is the azimuthal velocity magnitude contributed by the vortex, and $\boldsymbol{e}_\theta$ is a unit vector in the azimuthal direction. Substituting this into the modified momentum Eq. (2), in a frame convecting with $\boldsymbol{q}_\infty$, we have

$$\partial_t \boldsymbol{q} = \mu \nabla^2 \boldsymbol{q} - \epsilon \boldsymbol{n} \times \boldsymbol{\omega} \tag{11}$$

If $\epsilon = 0$, the solution is

$$T = [T_0/r]\left(1 - e^{-r^2/2\mu t}\right) \tag{12}$$

where T_0 is a constant. This, of course, results in a continually spreading vortical region with radius proportional to $\sqrt{2\mu t}$ and no nontrivial steady solution exists.

When $\epsilon > 0$, the steady solution of Eq. (11) with $\partial_t \boldsymbol{q} = 0$ for any positive value of μ and ϵ is

$$T = [T_0/r][1 - (1 + r/a)e^{-r/a}] \tag{13}$$

where $a = \mu/\epsilon$ is a length scale. The existence of the steady solution shows that the added confinement term effectively balances the diffusion by convecting the vorticity back toward the vortex center.

Numerical Implementation

The vorticity capturing method is implemented with two distinctive flow solvers in the present study. The first solver implemented in the ZETA code is based on a vorticity–velocity formulation and has been used extensively in the past for studies of many practical problems, including airfoil dynamic stall, Weis–Fogh problems of bio-fluid-dynamics, multi-element airfoil aerodynamics, and others. A manual for the flow solver is documented in Ref. 10, which contains detailed mathematical and numerical formulations. Basically, the solver first solves the vorticity transport equation by using an implicit finite difference method. This advances the vorticity field from the previous time level to a new level. The velocity at the new time level is then computed by an integral formulation[11] that is similar to the Biot–Savart law.

With the present vorticity confinement method, the velocity is modified after the velocity is computed by the ZETA code at each time level. The modification of the velocity field is accomplished by calling a separate module named CONFINE that computes the confinement term described by Eqs. (3–6). The module is developed such that it is self-contained and computationally efficient. The only requirement for the module is the specification of the grid and the velocity field from the basic flow solver. In the basic solver (ZETA code), after the velocity has been modified, the vorticity field corresponding to the modified velocity field is calculated. This corrected

vorticity field is then used to compute the final velocity field using the velocity integral formulation such that the mass balance is enforced. In the present study, the dynamic stall of a NACA 0012 airfoil and the interaction of a passing vortex with the airfoil are numerically investigated with and without the vorticity confinement.

The second effort of the present study involves the development of three-dimensional flow solver using the velocity–pressure formulation. In the basic solver, named VORD, the velocity is first convected by a split-velocity scheme.[12] The next step in the flow solver involves a multigrid scheme to solve a velocity potential Poisson equation derived from the continuity equation. The solution of the Poisson equation corrects the convected velocity field such that mass balance and the tangency condition on the solid surface are enforced. The two steps advance the velocity field from an old time level to a new time level. The pressure can be easily computed from the converged solution of the Poisson equation.

With the vorticity confinement, the velocity is modified after it has been convected, as described earlier with the ZETA code. The modification is accomplished by a call to the separate module CONFINE. Inviscid solutions of the interaction problem between passing vortex system and a circular cylinder were studied using the VORD code with and without the vorticity capturing.

Results and Discussion

Unsteady Navier–Stokes numerical results of a NACA 0012 airfoil were obtained for a dynamic stall and a vortex–airfoil interaction problem using the ZETA code. Unsteady inviscid numerical results for vortex–fuselage interaction problems were obtained using the VORD code. The solutions with vorticity capturing are compared with the basic solutions that were obtained by switching off the call to the module CONFINE.

Dynamic Stall

Figure 1 shows a fine grid region around a NACA 0012 airfoil and a coarse grid region enclosing the fine grid region. The overall grid is an O-grid with 81 grid lines in circumferential direction and 61 in the normal direction. For solutions with vorticity confinement, the confinement correction is not computed in the fine grid region where the numerical diffusion is small. The flow Reynolds number based on the freestream velocity and the airfoil chord is 1×10^6. Fully turbulent flow is assumed, and the Baldwin–Lomax algebraic model[13] is used. The airfoil oscillates about its quarter-chord between 5 and 25 deg angle of attack with a reduced frequency of 0.15 (normalized by the freestream velocity and the half-chord length). Fully developed numerical solutions at a constant angle of attack of 5 deg were first obtained before the airfoil started the oscillating motion.

Figure 2 shows load hysteresis loops of the oscillating airfoil for over one cycle. During the first cycle, the lift coefficient at the

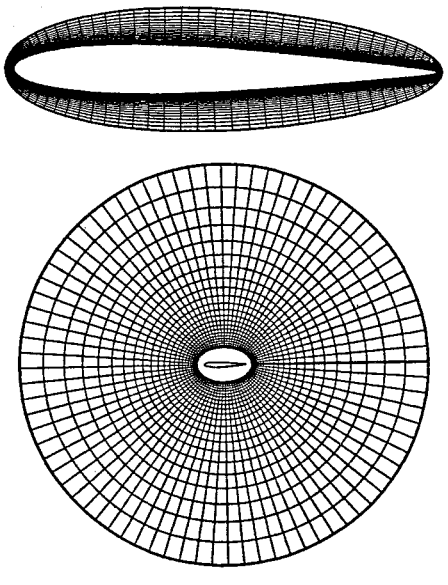

Fig. 1 Computational grids.

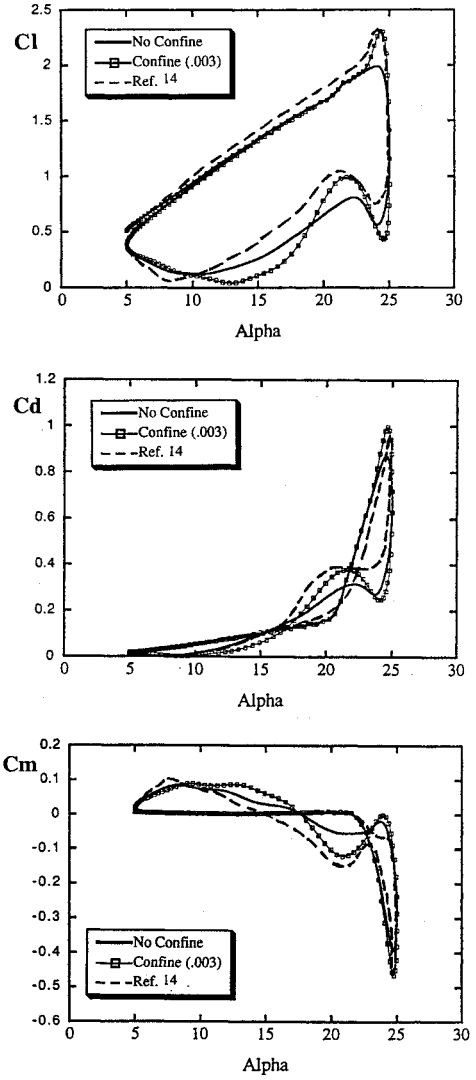

Fig. 2 Hysteresis loops for NACA 0012 airfoil; reduced frequency = 0.15, Reynolds number = 1×10^6.

beginning of the cycle is higher than during the second cycle. There are no differences in the lift coefficient for the two cycles when the angle of attack exceeds 13 deg during the airfoil upstroke. Without the vorticity confinement, the lift coefficient, represented by "no confine" in the figure, reaches approximately 2.0 and then starts to stall. With vorticity confinement, before the stall, the lift begins to rise at a much faster pace starting at 23 deg of the angle of attack. Compared with the "no confine" lift curve, the extra increase of lift is attributable to the stronger leading-edge separation bubble resulting from the vorticity confinement. This increase in lift is also observed experimentally in wind-tunnel tests,[14] also shown in the figure. The lift stall is followed by a lift increase that is caused by the formation and growth of another leading-edge separation bubble but with weaker strength. Comparing the two computational lift loops, the amplitude of the lift change is larger for the confined solution. In other words, the numerical diffusion dampens the strength of the separation vortices and therefore decreases the amplitude of the lift change during the oscillation cycle. It should be pointed out that the lift coefficient is almost identical for the two solutions during the airfoil upstroke before 23 deg of the angle of attack where the vorticity around the airfoil is mostly restricted to a thin layer, even where the flow has a reversed region on the airfoil upper surface.

Similar behavior is observed for the drag and the pitching moment hysteresis loops, also shown in Fig. 2. The computed instantaneous streamlines observed in the airfoil rotating frame are shown in Fig. 3 for the basic solutions and in Fig. 4 for the confined solutions. These figures clearly show that, except at 22.97 deg during the upstroke, the solutions with the vorticity confinement exhibit stronger separation

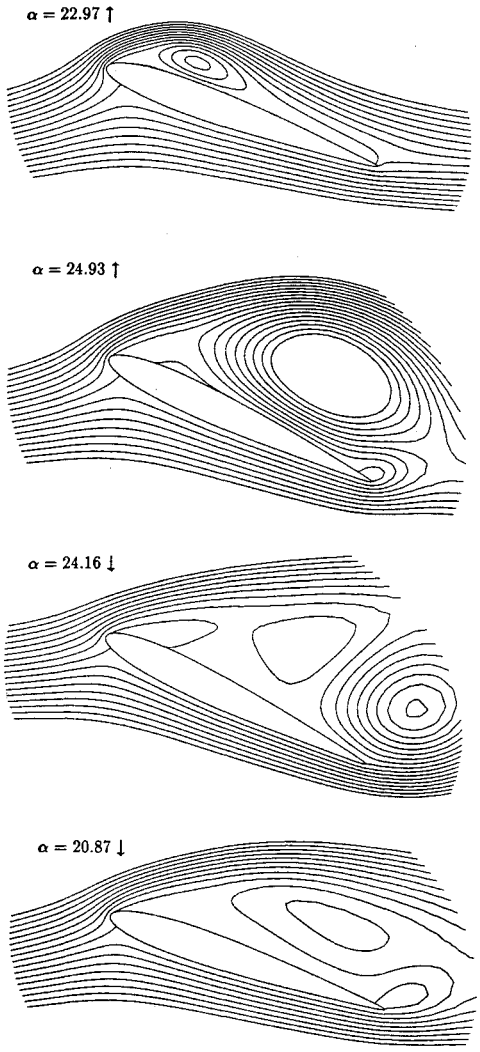

Fig. 3 Instantaneous streamlines, basic solution.

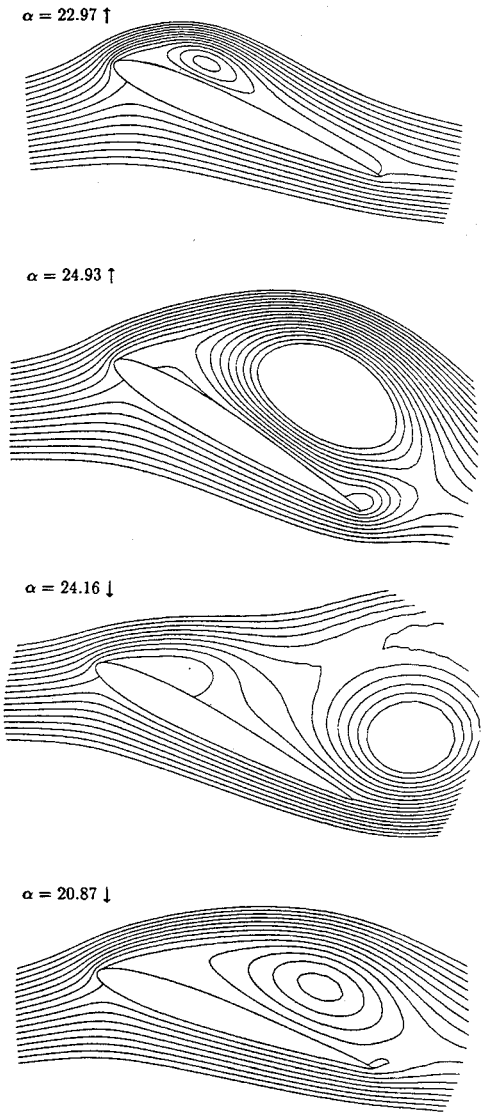

Fig. 4 Instantaneous streamlines, confined solution.

vortices. In the present computation, a value of 0.003 was used for ϵ of the confinement term. The effect of ϵ on the aerodynamic loads was studied by using different values of ϵ, and the results were presented in Ref. 15. When ϵ is within a rather wide range, the exact value ϵ has little effect on the aerodynamic loads. This phenomenon is also observed in a study of vortex sheet roll-up.[16] When ϵ is too large, unphysical flow solutions may result.

Vortex–Airfoil Interaction

A vortex is introduced upstream of a NACA 0012 airfoil, and the vortex is then convected with the local flow. The airfoil has an angle of attack 0.1 deg and the flow Reynolds number is 1×10^6. The same grid is used as in the dynamic stall case. The passing vortex, with an initial axisymmetric vorticity distribution, has a circulation of -0.2 (clockwise) normalized with the freestream velocity and the airfoil chord. In the present study, the release point of the passing vortex is one chord upstream and 0.26 chord below the airfoil camber line.

Converged flow solutions were first obtained for the airfoil without the passing vortex. Immediately after the release of the vortex, the time is set to start from zero. This time is normalized with the freestream velocity and a unit length. In this study, the airfoil has a chord length of 3.6 units. Figure 5 shows the equivorticity contours for the basic solution. In the figure the contour lines of the passing vortex extend from 30% of the original maximum vorticity. Without confinement, the passing vortex diffuses quickly, and by the time $T = 1.2$ almost all of the vorticity values above 30% of the original maximum have disappeared. With the confinement term, the obtained equivorticity contours are shown in Fig. 6. It can be seen

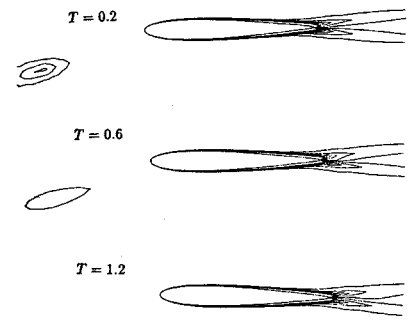

Fig. 5 Equivorticity contours, basic solution.

that the passing vortex retains its identity even at $T = 8.2$ where the vortex has already passed the airfoil trailing edge. A value of 0.02 was used for ϵ in this case.

Load variations are shown in Fig. 7. In this figure, the curve denoted by "single vortex" represents the solution of a passing point vortex with the same strength of circulation, with the vortex released at the same location as the distributed vortex. The decrease of the lift as the point vortex approaches the airfoil is caused by the decrease of the effective angle of attack resulting from the induced velocity field of the passing vortex. The following sudden increase of the lift is attributable to the point vortex located directly beneath the airfoil. With the unconfined, distributed vortex solution, the salient feature of the lift variation is not present, and the lift only stays

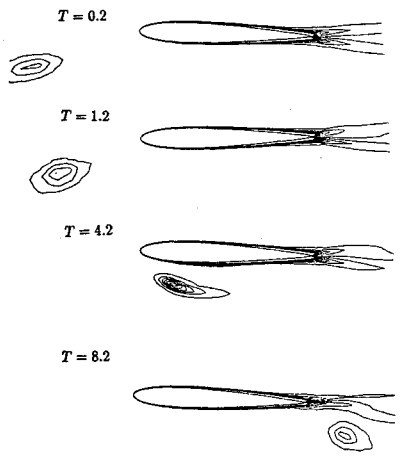

Fig. 6 Equivorticity contours, confined solutions.

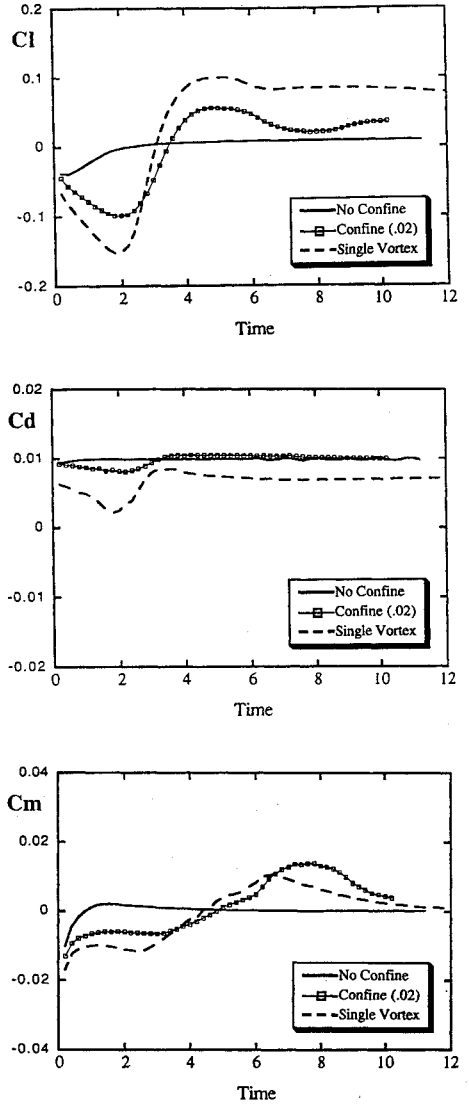

Fig. 7 Aerodynamic loads for vortex–airfoil interaction; passing vortex strength = 0.2.

low shortly and increases monotonically towards its steady value. This is simply the value without the presence of the passing vortex. With vorticity confinement, the salient feature of the (point) vortex–airfoil interaction is retained. The differences between the confined solution and the single vortex solution are caused by the finite size of the distributed passing vortex. Similar behavior is observed for the drag and pitching moment coefficients, also shown in Fig. 7.

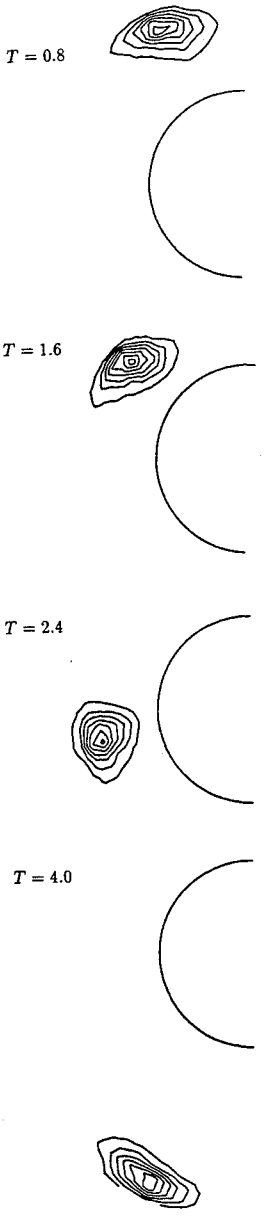

Fig. 8 Equivorticity contours, confined solution.

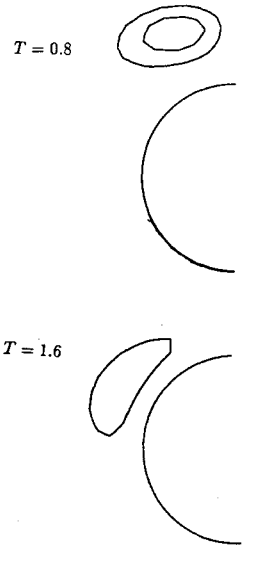

Fig. 9 Equivorticity contours, basic solution.

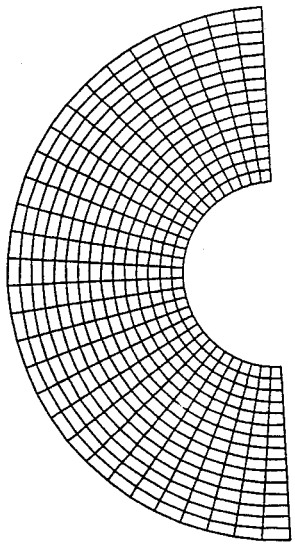

Fig. 10 Grid on one plane normal to cylinder axis.

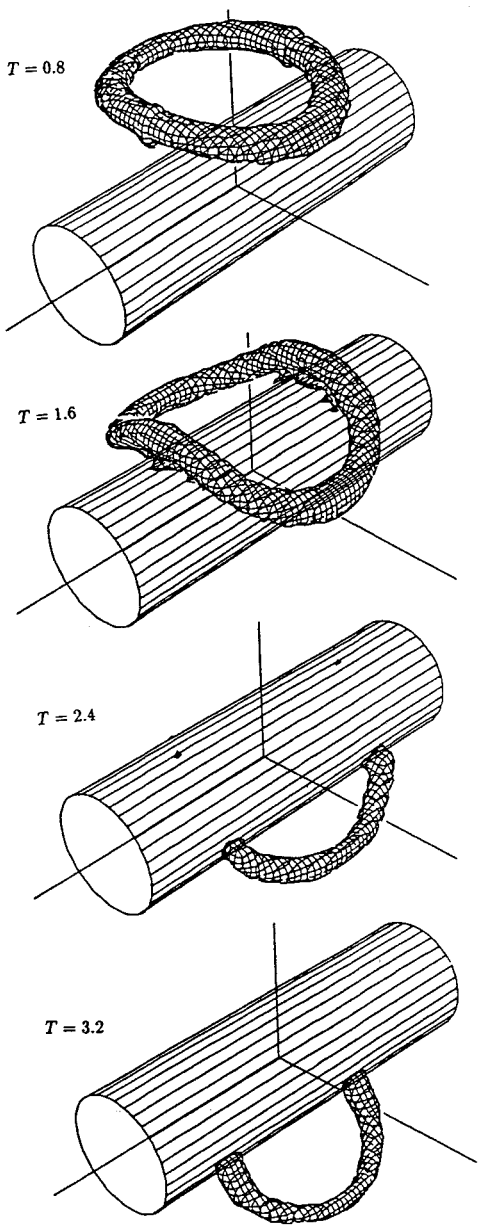

Fig. 11 Downward convection of vortex ring, confined solution.

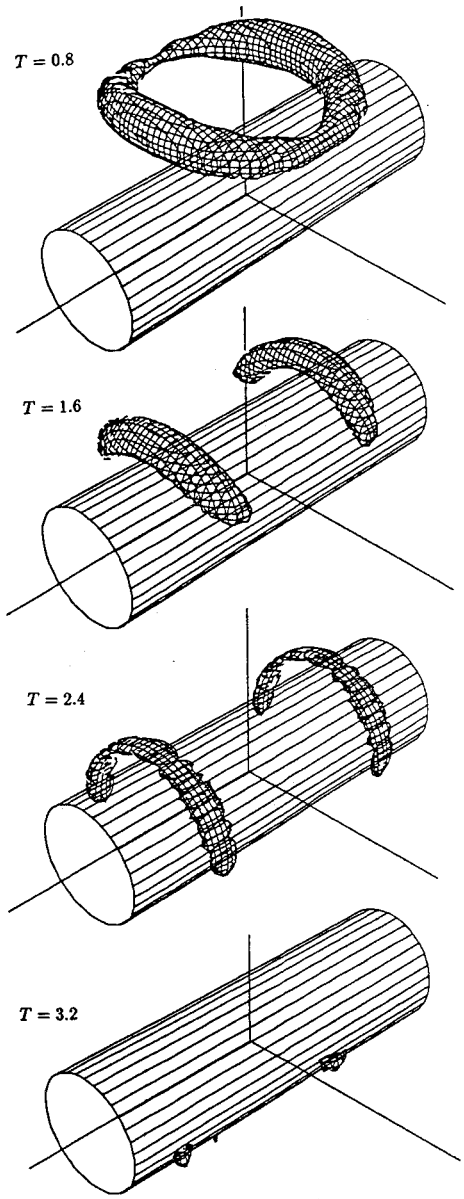

Fig. 12 Downward convection of vortex ring, basic solution.

Vortex–Fuselage Interactions

The rotorcraft fuselage is represented by a circular cylinder of infinite axial length in the present study. Unsteady three-dimensional inviscid solutions were obtained using the incompressible Euler solver VORD with and without vorticity confinement. For solutions with vorticity confinement, the velocity correction is computed in the entire flow domain. The first case computed involved a line vortex passing closely by the circular cylinder in an otherwise uniform downflow. In Fig. 8 contour plots of vorticity are presented for a sequence of time levels. The contours have the same value in each plot, extending from about 30% of the original maximum value. The figure shows that the vortex does not diffuse. In this case, a value of 0.02 was used for ϵ. Plots corresponding to the first two time levels are shown in Fig. 9 for results without vorticity confinement. The large effects of the numerical diffusion inherent in the basic numerical method are obvious. The computational grid is shown in Fig. 10.

The second computed case involves a vortex ring passing over the cylinder. (Solutions involving interacting vortex rings are presented in Ref. 9.) The vortex ring is initially positioned above the cylinder in an otherwise uniform downflow. A computational grid of $33 \times 33 \times 65$ is used, where the three members denote the number of points in the axial, radial, and circumferential directions, respectively. Figure 11 shows the vorticity surface of the confined solution at time levels $T = 0.8$, 1.6, 2.4, and 3.2. The vortex ring is displayed

by an iso-surface of vorticity magnitude of 20% of the maximum value of the initial vortex. At the same time levels, the iso-vorticity surface of the basic (unconfined) solution is shown in Fig. 12. In this figure, the iso-vorticity surface value is only half of the value in Fig. 11. The basic solution at $T = 0.8$ already shows effects of the numerical diffusion, particularly at locations away from the solid surface, where the grid is coarser. At $T = 1.6$ the vortex ring has impinged on the body and is beginning to stretch over it. Large parts of the vorticity surface disappear in the unconfined solution due to the numerical diffusion, whereas the confined solution at this time preserves the vorticity.

At $T = 2.4$, the vortex ring continues to stretch over the body, and the confined solution shows that vorticity closely interacts with the body surface. The velocity on the body surface is determined such that the boundary condition forces the vorticity tangential components of the vorticity to be zero. The flow tangency is then enforced by the solution of the velocity potential Poisson equation. This condition results in the vorticity impinging normal to the surface. At $T = 3.2$, the disappearance of the vortex contour surface of the unconfined solution indicates that the maximum value of the entire vortex structure is less than 10% of the initial maximum value. The contours of the confined solution show that the vortex structure is well preserved, where the ring has stretched over and almost reaches the bottom of the cylinder. The peak vorticity value at this final time level is still close to its initial value. The confined solution clearly demonstrates the ability of the vorticity confinement method to preserve the vortex ring structure with essentially no numerical diffusion.

Concluding Remarks

The present paper has demonstrated that the vorticity confinement method eliminates numerical diffusion effectively in problems involving vortex-dominated flows. Even though the basic flow solvers involved simple low-order convection schemes, the problem associated with large numerical diffusion in coarse grid regions was treated successfully with the new method. In the new technique, the confinement term is proportional to a single parameter ϵ, whose value was constant in each computed case. The term also depends on grid size and grid aspect ratio. It automatically becomes small in regions where the grid is fine so that viscous effects are correctly simulated. There, the numerical diffusion is small so that the confinement is not needed. Even though the constant ϵ used here is effective, further investigation of the implementation of the confinement term should lead to more robust problem-independent usage of the new method. The new method can be easily incorporated into existing Euler/Navier–Stokes flow solvers.

Acknowledgments

The present work was supported by U.S. Army and NASA contracts. Considerable guidance and support were given by Frank Caradonna and Paul Stremel of NASA Ames Research Center.

References

[1]Rai, M. M., "Navier–Stokes Simulations of Blade-Vortex Interaction Using High Order Accurate Upwind Schemes," AIAA Paper 87-0543, Jan. 1987.

[2]Oden, J. T., Strouboulis, T., and Devloo, P., "Moving-Grid Finite Element Algorithm for Supersonic Flow Interaction Between Moving Bodies," *Computational Methods in Applied Mechanical Engineering*, Vol. 59, 1986, pp. 327–362.

[3]Strawn, R. C., "Wing Tip Vortex Calculation with an Unstructured Adaptive Grid Euler Solver," 47th Forum of the American Helicopter Society, Phoenix, AZ, May 1991.

[4]Moore, D. W., "A Numerical Study of the Roll-Up of Finite Vortex Sheet," *Journal of Fluid Mechanics*, Vol. 63, Pt. 2, 1974, pp. 225–235.

[5]Hoeijmakers, W. M., and Vaatstra, W., "A Higher Order Panel Method Applied to Vortex Sheet Roll-Up," *AIAA Journal*, Vol. 21, No. 4, 1983, pp. 516–523.

[6]Steinhoff, J. S., and Ramachandran, K., "A Vortex Embedding Method for Free-Wake Analysis of Helicopter Rotor Blades in Hover," *Vertica*, Vol. 13, No. 2, 1989, pp. 133–141.

[7]Steinhoff, J. S., Wenren, Y., Mersch, T., and Senge, H., "Computational Vorticity Capturing: Application to Helicopter Rotor Flow," AIAA Paper 92-0056, Jan. 1992.

[8]Steinhoff, J. S., Thomas, M., and Wenren, Y., "Computational Vorticity Confinement: Two Dimensional Incompressible Flow," SECTAM XVI Conference, Nashville, TN, 1992.

[9]Steinhoff, J. S., and Underhill, D., "Modification of the Euler Equations for 'Vorticity Confinement': Application to the Computation of Interacting Vortex Rings," *Physics of Fluids*, Vol. 6, No. 8, 1994, pp. 2731–2744.

[10]Patterson, M. T., Wu, J. C., and Wang, C. M., "ZETA—A Manual for a Computer Code That Uses a Zonal Procedure for Evaluating Turbulent and Laminar Flows," Georgia Inst. of Technology, Atlanta, GA, Nov. 1987.

[11]Wu, J. C., and Wang, C. M., "Recent Advances of Boundary Element Method Formulation of Unsteady Viscous Flows," *Nonlinear Boundary Element Methods in Flow Problems*, edited by P. K. Banerjee and L. Morino, Elsevier Applied Science Publishers, Essex, England, UK, 1990, Chap. 7.

[12]Kim, J., and Moin, P., "Application of a Fractional-Step Method to Incompressible Navier–Stokes Equations," *Journal of Computational Physics*, Vol. 59, No. 2, 1985, pp. 308–323.

[13]Baldwin, B., and Lomax, H., "Thin Layer Approximation and Algebraic Model for Separated Turbulent Flows," AIAA Paper 78-0257, Jan. 1978.

[14]McAlister, K. W., Pucci, S. L., McCroskey, W. J., and Carr, L. W., "An Experimental Study of Dynamic Stall on Advanced Airfoil Sections, Pressure and Force Data," NASA TM 84245, Vol. 2, Sept. 1982.

[15]Wang, C. M., and Steinhoff, J. S., "Vorticity Capturing for Vortex-Dominated Flows," *Proceedings of Pacific International Conference on Applied Science and Technology* (PICAST) 1, Tainan, Taiwan, ROC, Dec. 1993.

[16]Steinhoff, J. S., Wenren, Y., Mersch, T., and Underhill, D., "Computational Vorticity Confinement: A Non-Diffusive Eulerian Method for Vortex-Dominated Flow," Univ. of Tennessee Space Inst., UTSI Preprint, Tullahoma, TN, May 1992.